Vacuum 146 (2017) 562–569

Contents lists available at ScienceDirect

Vacuum

journal homepage: www.elsevier.com/locate/vacuum

# First principles modeling of 3*d*-metal doped three-layer fluorite-structured $TiO_2$ (4,4) nanotube to be used for photocatalytic hydrogen production

Dmitry Bocharov [a, *], Sergei Piskunov [a], Yuri F. Zhukovskii [a], Eckhard Spohr [b], Pavel N. D'yachkov [c]

[a] Institute of Solid State Physics, University of Latvia, Riga, Latvia
[b] Department of Theoretical Chemistry, University of Duisburg-Essen, Germany
[c] Kurnakov Institute of General and Inorganic Chemistry, Russian Academy of Science, Moscow, Russia

ARTICLE INFO

*Article history:*
Received 4 January 2017
Received in revised form
27 April 2017
Accepted 1 May 2017
Available online 2 May 2017

*Keywords:*
Fluorite-structured titania nanotubes
Photocatalysis
Band-gap engineering
Linearized augmented cylindrical waves
Linear combination of atom-centered gaussian-type orbitals

ABSTRACT

We have estimated theoretically the photocatalytic suitability of thinnest single-wall fluorite-structured titania (4,4) nanotube (NT) possessing three layers each (O-Ti-O) and doped by Sc, V, Cr, Mn, Fe, Co, Ni, Cu and Zn atoms substituted for host Ti atoms. For this goal, we have performed large-scale *ab initio* calculations on $TiO_2$ NTs with three-layer morphology doped by 3*d* transition metals, using (*i*) the method of linear combination of atom-centered Gaussian-type orbitals (LCAO) based on the hybrid density functional theory (DFT) incorporating the Hartree-Fock (HF) exchange contribution (DFT+HF) and (*ii*) the method of linearized augmented cylindrical waves (LACW) with the muffin-tin approximation based on the local density functional approach (LDA). We have compared the ground state electronic structure, particularly the one-electron densities of states (DOSs) from the LCAO and LACW calculations for periodic arrangements of the 3*d*-metal dopant atoms. The results show clear evidence for a potential photocatalytic application for water splitting in the case of the Sc-doped titania nanotubes only. These NTs show both a reduced band gap of 2.0 eV relative to the pristine NT and an absence of defect-induced levels between the redox potentials of hydrogen and oxygen, so that electron-hole recombination becomes unlikely. Other 3*d* dopants with higher atomic number, although their band gap also covers the favorable green to orange region of the solar spectrum, are unsuitable because their defect-induced levels are positioned between the redox potential of oxygen and hydrogen, which can be expected to lead to rapid electron-hole recombination.



## 1. Introduction

The discovery of $H_2O$ photolysis on a $TiO_2$ electrode [1] was an important event in the development of electrochemical splitting of water or aqueous solutions under the influence of solar irradiation, which releases molecular hydrogen. Because of the chemical activity of $TiO_2$ (titania), its high stability, nontoxicity and low cost, this photocatalytic material has attracted much attention during the last two decades. However, its application in the field of renewable energy and ecological environmental protection is limited by the large value of optical gap $\Delta\varepsilon_{gap}$ of stable $TiO_2$ crystalline phases (3.2 eV for anatase- and 3.0 eV for rutile-structured titania [2]). Due to the wide band gap, this compound utilizes only a few percent of solar light in the UV range for photocatalysis, while almost half of the solar energy is emitted in the visible light range [3]. Thus, to make progress in the utilization of $TiO_2$ photocatalysts one must find ways to extend effectively the spectral $TiO_2$ response to the visible light region.

Electronic band modification is a promising way to extend the absorption edge of the $TiO_2$ [4–7] and possible by doping titania crystals with several 2*p* and 3*p* non-metal elements (C, N, F, and S) or by doping with transition 3*d*-, 4*d*-, and 5*d*-metal elements. The doping can either insert an impurity band into the original band gap, or it can modify the conduction or valence band somewhat, thereby improving the conditions for photocatalytic activity of the crystal. *Ab initio* calculations on the electronic structure of the

* Corresponding author.
*E-mail address:* bocharov@latnet.lv (D. Bocharov).

http://dx.doi.org/10.1016/j.vacuum.2017.05.002
0042-207X/

titania crystals show that, particularly, Sc, V, Cr, Mn, Fe, Co, Ni, Cu, and Zn 3*d*-metal dopants produce mid-gap states [8–15].

At the same time, a more effective way to improve the photocatalytic activity of titania was found to be the reduction of its dimensionality from 3D crystalline bulk to $TiO_2$ 2D nanothin sheets or to 1D nanotubes. These materials possess, in addition, large surface areas and unique shapes with few interfacial grain boundaries, which promote charge transport and electron-hole pair separation [16]. Nano-tubular $TiO_2$ can be prepared by the hydrothermal method, *via* a sol–gel process, or when the carbon nanotubes (CNTs) being used as templates for titania growth, and a few others [17–23]. It has been found recently that NT surface structure, shape and diameter could be controlled for arrays of anodized $TiO_2$ nanotubes when applying an electric field [24].

Transformation of bulk to the nanotubes *via* formation of nanosheets can be expected to lead to an unfavorable growth of the band gap due to confinement effects, which, however, can fortunately be compensated or even used advantageously by implementation of transition metal dopants in NT using the ion-exchange technique with band gap states.

There are seven structural types of titania crystals, the majority of which are metastable [25]. Similar to the formation of minimum-thick CNTs from a graphene sheet, fluorite-type $TiO_2$ NTs can be constructed by rolling-up stoichiometric three-layer O-Ti-O nanosheets initially formed from more stable rutile (110) or anatase (101) slabs. The geometry optimization of three-layer anatase-structured O-Ti-O (101) slab spontaneously transforms it to a centered hexagonal (111) fluorite-structured nanosheet, which can be rolled up to form single-wall (SW) NTs with either armchair- or zigzag-type chirality [26,27].

The main purpose of the current study is to calculate the electronic structure of morphologically simple hexagonal $TiO_2$ nanotubes (which are metastable due to their extremely thin thickness), doped by 3*d* metal atoms. As it was shown in Ref. [28], when using DFT+*U* method, transition metal doping of titania anatase-structured crystals results in a reduction of the band gap. The number of experimental studies of $TiO_2$ nanostructures doped by 3*d* metal atoms is quite small. The efficiency of Sc-doped anatase nanoparticles was found to be 6.7% larger than the efficiency of dye-sensitized solar cells with pure anatase [29]. On the other hand, the conditions of synthesis are extremely important for photocatalytic properties of experimentally synthesized nanomaterials. In Refs. [30,31], Sc-doped and V-doped $TiO_2$ show lower photocatalytic activity as compared to non-doped anatase, which can be associated with a presence of metal oxide islands covering the reactive sites of Sc-doped $TiO_2$, and thus increased electron-hole pair recombination [31]. The photocatalytic activity of Rhodamine B caused by oxidation of $TiO_2$ NTs doped by Ag, Al, Mn, Ni and Zn was studied in Ref. [32] indicating preferable photocatalytic suitability of Zn-doped nanotubes.

With the goal in mind to obtain unbiased information and to estimate the importance of theoretical simulations, we have applied two different *ab initio* techniques, namely, the method of the linear combination of atomic orbitals (LCAO) with Gaussian-type orbitals [33,34] and the method of linearized augmented cylindrical waves (LACW) [35,36]. Previously, we studied the structural stability and the electronic band structure for pristine single- and multi-layer fluorite as well as anatase-type $TiO_2$ nanotubes with first-principle quantum chemistry [16,26,27,37,38]. The photocatalytic suitability of C, Fe, N, and S doped (*e.g.*, N+S co-doped) anatase-structured $TiO_2$ NTs with either the [001] or the [101] orientation of the chiral vectors was evaluated by us theoretically too [16,39–42]. In the present study, all calculations have been performed to estimate the suitability for the particular case of 3*d*-metal doped fluorite-structured (4,4) $TiO_2$ SW NTs with 24 atoms *per* translational unit cell (Fig. 1).

The paper is organized as follows. Models of pristine and doped fluorite-type (4,4) titania nanotubes as well as methods used to calculate their structural, electronic and photocatalytic properties are given in Section 2. Section 3 contains the analysis of $TiO_2$ SW NT features obtained from the Gaussian-basis LCAO method, a comparison of the LCAO- and LACW-simulated total and projected densities of states, and a comparative analysis of the photocatalytic capabilities of NTs under study. Obtained results are summarized in Section 4.

## 2. Theoretical background

### 2.1. Atomistic model of single-walled fluorite-structured (4,4) titania nanotube

Three-layer titania nanosheets with the hexagonal fluorite-type (111) structure can be rolled up to form 3-layer titania SW NTs with either (*i*) armchair-type (*n*,*n*) chirality or (*ii*) zigzag-type (*n*,0) chirality [26,27]. For our simulations, we have chosen the former with $n = 4$ (Fig. 1).

### 2.2. LCAO calculations

When constructing a 1D periodic model of SW nanotubes using CRYSTAL code [34], the formalism of periodic rototranslation symmetry has been exploited successfully. This approach has been applied earlier by us for simulations of perfect SW $TiO_2$ NTs belonging to either the anatase or fluorite type [26,27].

In the hybrid density functional theory approach, which incorporates an admixture of the Hartree-Fock exchange contribution (DFT+HF) together with the generalized gradient approximation (GGA), a modified B3LYP exchange-correlation functional [43] has been adopted by us for the LCAO calculations on both pristine and doped titania nanotubes. The reason for this approach is that it leads to a better reproduction of their atomic and electronic structure obtained earlier in experiments and theoretical simulations [39–42]. For the DFT-LCAO calculations, we have used the formalism of the localized Gaussian-type functions (GTFs), which form the basis set (BS) of atomic orbitals for each chemical element as implemented in the CRYSTAL code [34]. The following configurations of localized GTF functions have been adopted for

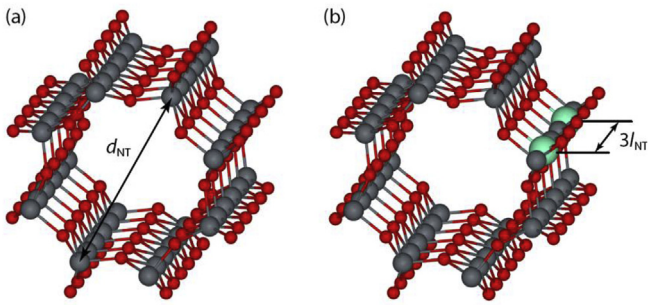


**Fig. 1.** Axonometric images of non-optimized pristine (a) and doped (b) armchair-type (4,4) fluorite-structured $TiO_2$ NT fragments containing three unit cells ($3l_{NT}$ corresponds to the tripled length of the unit cell). Small red, middle gray and large turquoise balls describe O, Ti, and 3*d*-metal dopant atom substituted for Ti atom, respectively. The nanotube diameter ($d_{NT}$), defined to be equal to the distance between two opposite Ti atoms inside one cross-layer of pristine NT (a) is 0.84 nm. The distance between the nearest dopant atoms along the NT axis is the tripled length of the nanotube unit cell ($l_{NT}$) containing 24 atoms *per* UC (8Ti+16O) (b). Thus, dopant concentration in considered fluorite-structured titania nanotubes equals to 4.17%. (For interpretation of the references to colour in this figure legend, the reader is referred to the web version of this article.)

further first principles calculations:

- full-electron BSs have been adopted: 8*s*–411*sp*–1*d* [40] for O atoms;
- the basis set has been chosen in the form 411*sp*–311*d* [40], using the effective core potentials (ECP) implemented by Hay and Wadt [44], for Ti atoms;
- the triple-zeta valence potentials (TZVP) in the form 842111*s*-6311*p*-411*d*-1*f* [45] for 3*d*-metal atoms considered as point dopants (except for Ti).

To achieve a quantitative agreement with the experimentally observed band gap for anatase-structured $TiO_2$ bulk ($\Delta\varepsilon_{gap}$ = 3.18 eV), the admixture of non-local HF exchange in the hybrid B3LYP functional defined by the DFT-GGA method has been reduced from the standard 20% [34] down to 14% [39]. To provide a balanced summation over the direct and reciprocal lattices of pristine and doped nanotubes, the reciprocal space integration has been performed by sampling the Brillouin zone (BZ) of extended 3 NT unit cells (Fig. 1) with the 6 × 1 × 1 Pack–Monkhorst *k*-mesh [46], which results in evenly distributed *k*-points over the segment of the irreducible BZ. The threshold parameters implemented in the CRYSTAL code ($ITOL_n$, where $n$ = 1–5) for evaluation of different types of bi-electronic integrals have been set to 7, 8, 7, 7, and 14, respectively (if the overlap between the two atomic orbitals is smaller than $10^{-ITOL_n}$, the corresponding integral was truncated). Calculations have been considered as converged when the total energy obtained in the self-consistent field procedure differed by less than $10^{-7}$ a.u. in two successive SCF cycles. Further increase of *k*-mesh and threshold parameters has resulted in much more expensive calculations yielding only a negligible change in the total energy.

### 2.3. LACW calculations

The LACW technique is an extension of the linearized augmented plane-wave (LAPW) method to the specific case of the one-dimensional cylindrical or tubular polyatomic systems like the fluorite structured titania nanotubes studied here (Fig. 1). The main foundations and applications of the LACW method are described in detail elsewhere [35,47–50] and are compiled in a recent review [36]. Here, we only list the basic approximations used in this theory. Similar to the original LAPW theory for bulk materials, the LACW method is based on a muffin-tin (MT) approximation for electronic potentials. That is, the potential $V(\mathbf{r})$ is constructed to be spherically symmetric in the regions of atoms and constant between them. However, there is a large difference between the bulk and nanomaterials, because electron transport is unlimited in all directions in the first case, while in nanotubes it is surely determined by their size and tubular shape. Therefore, the MT method is slightly adapted to the cylindrical structures. According to the cylindrical MT approximation, we consider the tubule to be positioned between the infinite barriers $\Omega_a$ and $\Omega_b$, which separate the polyatomic system from the vacuum regions outside and inside the NT. Similarly to the APW/LAPW model, we also apply a $\rho(\mathbf{r})^{1/3}$ local density exchange potential, where the electron density $\rho(\mathbf{r})$ of the nanotube is calculated as a superposition of atomic densities. Inside the MT spheres, its spherically symmetric part $\rho(r)$ is taken. In the inter-spherical space, the potential $V(r)$ is taken as the energy zero point. As a result, the electronic structure of a nanotube is determined in the LACW method by free electron movement in the inter-spherical region between the barriers and by electron scattering from the atomic spheres.

To perform DFT-LACW calculations on both pristine and doped $TiO_2$ NTs, we have applied the formalism of the localized density approximation (LDA) [35,36]. Since the standard DFT-LDA methods evidently underestimate the energy band gap when using the cylindrical muffin-tin approximation [49], we have introduced an additional parameter, namely, the width $\Delta$ of cylindrical layer, which is the same for both the pristine and the doped $TiO_2$ NTs. In this paper, the parameter $\Delta$ = 4.06 Å has been chosen so that the energy band gap in the pristine fluorite structured $TiO_2$ nanotube is close to 4.0 eV, which is similar to the value obtained in DFT-LCAO calculations (Fig. 2 and Table 2, Subsection 3.2). Note that this value ($\Delta$) is almost the same as the van der Waals thickness of the $TiO_2$ layer, so that the area confined by barriers accommodates a significant part of the electron density in nanotube.

### 2.4. Formation energies for 3d-metal dopants

To estimate the ability of a dopant to form a point substitution defect in a fluorite-type single-walled $TiO_2$ NT, one has to perform LCAO calculations of the formation energies:

$$E^{form}_{A_h} = E^{tot}_{A_h/NT} + E^{tot}_{h} - E^{tot}_{A_h} - E^{tot}_{NT}, \quad (1)$$

where $E^{tot}_{A_h/NT}$ is the calculated total energy of nanotube containing substitutional $A_h$ atom, $E^{tot}_{h}$ is the total energy of the host Ti atom removed from the nanotube, $E^{tot}_{A_h}$ is the total energy calculated for the impurity 3*d*-metal atom, finally $E^{tot}_{NT}$ stands for the total energy calculated for the pristine $TiO_2$ NT. Obviously, a comparative analysis of the formation energies for different dopants and sites of their location within various substrates allows one to determine the energetically most favorable configurations of doped $TiO_2$ NTs for photocatalytic applications. However, the ultimate conclusion concerning their suitability can only be done properly when analyzing in detail their band structures and appearance of additional levels in the band gap, thus, creating, *e.g.*, new optical absorption edges.

### 2.5. Evaluation of photocatalytic suitability of 3d-metal doped titania nanotubes

For a photocatalytically efficient semiconductor, its band gap, *i.e.* the difference between the conduction band bottom ($\varepsilon_{CB}$) and the valence band top ($\varepsilon_{VB}$), must correspond to the visible light range [51]. In order to provide water splitting, both the oxidation and reduction potentials of a water molecule in solution ($\varepsilon_{O_2/H_2O}$ and $\varepsilon^{+}_{H/H_2}$, respectively, the difference between which was found to be 1.23 eV), must be positioned inside the band gap of the photocatalytic electrode [52]. Thus, $\Delta\varepsilon_{gap} = \varepsilon_{CB} - \varepsilon_{VB}$ must correspond to at least 1.5 eV, which corresponds to an energy range between both visible red and near infrared (IR) light. On the other hand, $\Delta\varepsilon_{gap}$ has to be narrower than 2.8 eV to allow a catalyst to utilize energy from the visible, violet, or near-ultraviolet (UV) light range. Since ultraviolet light accounts for about 4% of the total solar irradiation, the maximum efficiency of visible light for photocatalysis corresponding to the band gap of 2.0–2.2 eV width can be estimated to be about 20% [53]. For effective photocatalytic water splitting with hydrogen production, at least a rate of conversion above 10% is needed to compete against solar-cell-driven $H_2O$ electrolysis and to be economically profitable [54].

Doped crystalline species such as nanotubes can be characterized by the presence of impurity levels inside their band gaps [49]. In this case, the energy balance for possible water splitting under the effect of visible light photons can be improved due to decrease of the energy gap between the highest occupied and lowest

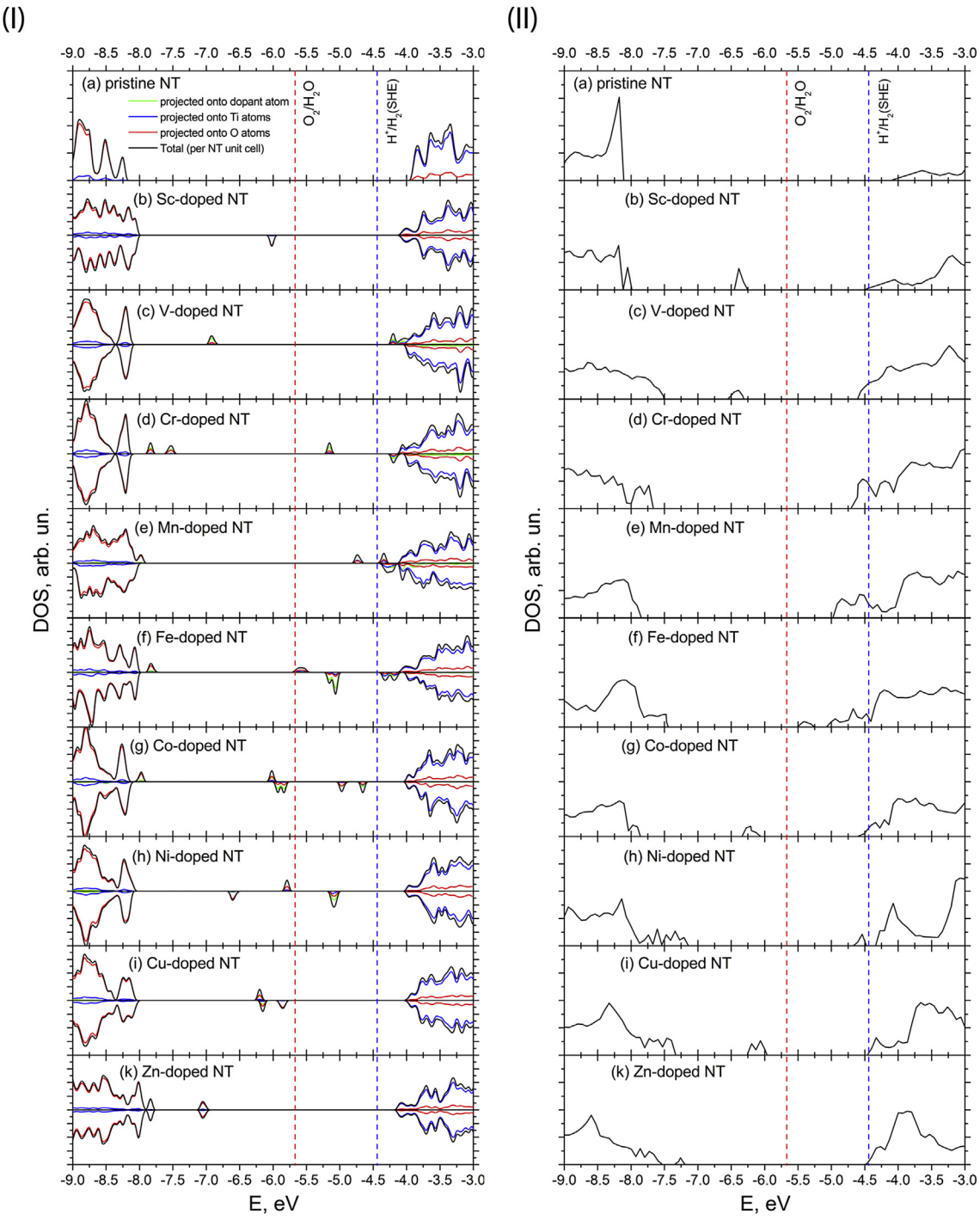


**Fig. 2.** Comparison of the densities of states (DOSs) for pristine (a) and doped by 3*d*-metal atoms (b-k) $TiO_2$ NTs, calculated using B3LYP-LCAO method (left vertical panel I) and LDA-LACW method (right panel II). For the former case, we construct total and partial DOSs projected on O, Ti and dopants (their profiles differ by colors as described in (Ia) inset). The zero value of the energy scale corresponds to the vacuum level. Vertical lines stand for $\varepsilon_{O_2/H_2O}$ (red) and $\varepsilon_{H^+/H_2}$ (blue) potentials. LCAO and LACW calculations on doped and pristine NTs have been performed using spin-polarized and spin-frozen techniques, respectively. (For interpretation of the references to color in this figure legend, the reader is referred to the web version of this article.)

unoccupied impurity levels ($\varepsilon_{HOIL}$ and $\varepsilon_{LUIL}$, respectively). At the same time, this new energy gap must include both the oxidation and the reduction potential of water, $\varepsilon_{O_2/H_2O}$ and $\varepsilon_{H^+/H_2}$, in order to protect the possible photocatalyst against both electron-hole recombination and photocorrosion [51]. The proper photocatalytic disposition of all induced levels inside the band gap has to follow the inequalities [40]:

$$\varepsilon_{VB} < \varepsilon_{HOIL} < \varepsilon_{O_2/H_2O} < \varepsilon_{H^+/H_2} < \varepsilon_{LUIL} < \varepsilon_{CB}. \quad (2)$$

Eq. (2) demonstrates that a reduced photon energy can be required for dissociation of $H_2O$ molecules in the proximity of doped semiconductor NTs as compared to the pristine one.

**Table 1**
Structural, electronic, and energy parameters of doped titania NTs with optimized geometry as calculated using the DFT-LCAO method. Here, $d_{NT}$ is the distance between the dopant atom and the opposite Ti atom across the NT; $3l_{NT}$ is the equilibrium distance between periodically repeated dopants; $l_{dopant\text{-}O}$ is the bond length between dopant and host oxygen atoms; $p_{dopant\text{-}O}$ is the population of dopant-host oxygen bonds; $q_{dopant}$, $q_O$ and $q_{Ti}$ are the net charges on the dopant atom, on the host O atom closest to the dopant, and on the host Ti atom closest to the dopant. The last column contains the formation energy *per* dopant atom ($E_{form}$, Eq. (1)).

| dopant | $d_{NT}$, Å | $3l_{NT}$, Å | $l_{dopant\text{-}O}$, Å | $p_{dopant\text{-}O}$, me | $q_{dopant}$, *e* | $q_O$, *e* | $q_{Ti}$, *e* | $E^{form}$, eV |
|---|---|---|---|---|---|---|---|---|
| pristine NT | 8.40 | 8.70 | 1.84 | 138 | – | −1.04 | 2.24 | – |
| Sc | 5.07 | 8.87 | 2.00 | 174 | 1.69 | −1.06 | 2.29 | 5.92 |
| V | 6.01 | 8.77 | 1.67 | 120 | 1.73 | −0.86 | 2.27 | 5.50 |
| Cr | 6.16 | 8.76 | 1.72 | 152 | 2.01 | −1.07 | 2.26 | 8.01 |
| Mn | 4.67 | 8.83 | 1.79 | 94 | 1.80 | −1.06 | 2.32 | 13.68 |
| Fe | 7.04 | 8.80 | 1.79 | 66 | 1.41 | −0.85 | 2.29 | 13.98 |
| Co | 5.95 | 8.76 | 1.81 | 48 | 1.60 | −1.02 | 2.27 | 15.94 |
| Ni | 6.34 | 8.77 | 1.91 | 126 | 1.27 | −1.01 | 2.27 | 16.11 |
| Cu | 6.49 | 8.75 | 1.86 | 142 | 1.64 | −1.08 | 2.26 | 14.77 |
| Zn | 7.60 | 8.85 | 1.94 | 170 | 1.38 | −0.82 | 2.25 | 19.94 |

**Table 2**
Edges of band gaps ($\varepsilon_{VB}$ and $\varepsilon_{CB}$) and widths of band gaps ($\Delta\varepsilon_{gap}$), as well as the highest occupied and lowest unoccupied levels induced by dopants ($\varepsilon_{HOIL}$ and $\varepsilon_{LUIL}$) and reduced band gaps ($\Delta\varepsilon'_{gap}$) between induced levels calculated using LCAO and LACW methods.

| discrete energies | (111) nanosheet | Pristine NT | dopants | | | | | | | | |
|---|---|---|---|---|---|---|---|---|---|---|---|
| | | | Sc | V | Cr | Mn | Fe | Co | Ni | Cu | Zn |
| *LCAO calculations* | | | | | | | | | | | |
| $\Delta\varepsilon_{gap} = \varepsilon_{CB} - \varepsilon_{VB}$ | | | | | | | | | | | |
| $\varepsilon_{VB}$, eV | −8.56 | −8.20 | −8.00 | −8.12 | −8.13 | −7.94 | −7.76 | −7.92 | −8.08 | −8.03 | −7.78 |
| $\varepsilon_{CB}$, eV | −4.73 | −3.86 | −4.00 | −4.17 | −4.15 | −4.27 | −4.37 | −3.91 | −3.88 | −3.83 | −4.18 |
| $\Delta\varepsilon_{gap}$, eV | 3.83 | 4.34 | 4.00 | 3.95 | 3.98 | 3.66 | 3.39 | 4.01 | 4.20 | 4.20 | 3.60 |
| *reduced band gaps $\Delta\varepsilon'$ in presence of induced levels* | | | | | | | | | | | |
| $\varepsilon_{HOIL}$, eV | −8.56 | −8.20 | −5.98 | −6.86 | −7.47 | −7.94 | −7.76 | −7.92 | −8.08 | −8.03 | −7.02 |
| $\varepsilon_{LUIL}$, eV | −4.73 | −3.86 | −4.00 | −4.17 | −5.12 | −4.71 | −5.60 | −5.99 | −6.65 | −6.17 | −4.18 |
| $\Delta\varepsilon'_{gap}$, eV | 3.83 | 4.34 | 1.98 | 2.69 | 2.35 | 3.23 | 2.17 | 1.93 | 1.43 | 1.86 | 2.84 |
| *LACW calculations* | | | | | | | | | | | |
| $\Delta\varepsilon_{gap} = \varepsilon_{CB} - \varepsilon_{VB}$ | | | | | | | | | | | |
| $\varepsilon_{VB}$, eV | – | −8.11 | −8.05 | −7.51 | −7.73 | −7.91 | −7.45 | −7.90 | −7.21 | −7.40 | −7.60 |
| $\varepsilon_{CB}$, eV | – | −3.64 | −4.50 | −4.56 | −4.61 | −4.91 | −5.01 | −4.51 | −4.27 | −4.40 | −4.46 |
| $\Delta\varepsilon_{gap}$, eV | – | 4.47 | −3.55 | 2.95 | 3.12 | 3.00 | 2.44 | 3.39 | 2.93 | 3.00 | 3.13 |
| *reduced band gaps $\Delta\varepsilon'$ in presence of induced levels* | | | | | | | | | | | |
| $\varepsilon_{HOIL}$, eV | – | −8.11 | −6.38 | −6.33 | −7.73 | −7.91 | −7.45 | −7.90 | −7.21 | −7.40 | −7.29 |
| $\varepsilon_{LUIL}$, eV | – | −3.64 | −4.50 | −4.56 | −4.61 | −4.91 | −5.46 | −6.27 | −4.61 | −6.20 | −4.46 |
| $\Delta\varepsilon'_{gap}$, eV | – | 4.47 | 1.88 | 1.77 | 3.12 | 3.00 | 1.99 | 1.63 | 2.60 | 1.20 | 2.83 |

## 3. Results and discussion

### 3.1. Geometry, electronic charge and formation energy of pristine and doped (4,4) $TiO_2$ NTs

Table 1 clearly shows that when comparing the values for pristine and doped fluorite-structured titania nanotubes all the substitutional atoms relax inwards into the nanotube: the largest decrease of the cross-section value, $d_{NT}$, as compared to its pristine *value* is observed for the Mn dopant (44.4%), the smallest one for the Zn atom (9.5%). Most likely, this effect particularly depends on the intensity of electron charge redistribution in the vicinity of the dopants. For example, the electron population $p_{dopant\text{-}O}$ of the dopant-host oxygen bond (describing its degree of covalency) essentially decreases for Mn-O and increases for Zn-O bonds as compared to arbitrary Ti-O bonds in the pristine NT.

On the other hand, the bond lengths, $l_{dopant\text{-}O}$, tend to be elongated with increasing atomic mass and correspondingly, atomic radius, of the substitutional 3*d* defect (with the exception of the lightest metal, Sc, for which the distance $l_{Sc\text{-}O} = 2.00$ Å is the largest, *cf.* $l_{Sc\text{-}O}$ with $l_{Zn\text{-}O} = 1.94$ Å and $l_{Ti\text{-}O} = 1.94$ Å in pristine NT). Other geometry and charge parameters of doped $TiO_2$ NTs ($l_{NT}$, $q_{dopant}$, $q_O$ and $q_{Ti}$) in the 3*d*-metal period (Table 1) are not too sensitive with respect to the positions of 3*d* dopant elements in the Periodic Table and have rather random values.

The formation energies of the point substitutional impurities in a relaxed titania nanotube are observed to grow consequently with increasing atomic number of 3*d* metal dopants, except for Sc and Cu. At the same time, the high values of $E^{form}$ for the majority of 3*d*-metal doped $TiO_2$ NTs (excluding Sc, V and Cr, Table 1) make them energetically inefficient even for metastable fluorite-structured titania nanotubes, thus, their possible suitability for photocatalytic applications is rather doubtful. Nevertheless, we analyze below the corresponding densities of one-electron states (DOSs) presented in Fig. 2 in order to make definite conclusions.

### 3.2. Total and projected DOSs of nanotubes calculated using LCAO and LACW methods

Table 2 shows that the band gap of the pristine titania nanotube noticeably exceeds those of the (111) nanosheet, as it was also observed earlier for both anatase- and fluorite-structured single-walled $TiO_2$ NTs [26]. Doping of nanotubes essentially reduces the $\Delta\varepsilon'$ values as well as the $\varepsilon_{CB}$ edges (the shifts of the $\varepsilon_{VB}$ edges are found to be more smooth). All doped $TiO_2$ NTs have been studied at the initial inter-defect distance of 8.7 Å (Fig. 1b and Table 1), corresponding to the triple length of the NT unit cell ($3l_{NT}$). The interaction between the adjacent 3*d* dopants along nanotube has been found to be negligible since the energy dispersion of the populated induced levels in the calculated band structures of defective titania nanotubes does not exceed 0.03 eV.

To evaluate the photocatalytic suitability of doped $TiO_2$ NTs, we

have checked fulfillment of the following conditions: (*i*) agreement with Eq. (2), (*ii*) disposition of the reduced band gap inside the energy range of solar light (1.5 eV < $\Delta\varepsilon'_{gap}$ < 2.8 eV), and (*iii*) the absence of overlap between the induced levels and the interval between the oxidation and reduction potentials ($\varepsilon_{HOIL}$ < −5.76 eV and −4.44 eV < $\varepsilon_{LUIL}$). Although certain constraints for these conditions might exist, both Table 2 and Fig. 2 allow us to estimate the potential suitability of doped single-walled fluorite-type titania nanotubes for use in photocatalytic applications.

The B3LYP-LCAO calculations on both pristine and doped titania nanotubes allow us to perform orbital analysis of projected densities of states (Fig. 2I), e.g., to clarify their natural chemical composition. In the case of the pristine $TiO_2$ NT, the top of the valence band is predominantly formed by the O (2*p*) orbitals with small contributions from Ti (3*d*) ones, while the bottom of the conduction band is formed by Ti (3*d*) states and a less visible contribution of O (2*p*) states. On the other hand, the energy levels induced by 3*d*-metal dopants have a different nature: (*i*) in the Sc-doped NT, its occupied $\varepsilon_{HOIL}$ level is mainly populated by O (2*p*), while in the case of the Zn-doped nanotubes, the induced levels can correspond either to the occupied $\varepsilon_{HOIL}$ level or to the unoccupied $\varepsilon_{LUIL}$ level which is instable and can easily be filled during initial excitation; (*ii*) in the NTs doped by the remaining 3*d* metal atoms (Me = V, Cr, Mn, Fe, Co, Ni and Cu), the induced levels contain mainly Me (3*d*) state contributions from the same dopant atoms, however, the V-doped level is occupied with $\varepsilon_{LUIL} = \varepsilon_{CB}$ while for other dopants, the induced levels are positioned between the redox levels $\varepsilon_{O_2/H_2O}$ and $\varepsilon_{H^+/H_2}$, which indicates a high possibility of electron-hole recombination in the doped nanotube.

### 3.3. Comparison of LCAO- and LACW-represented energy plots for doped $TiO_2$ NTs

A schematic representation of the band gap edges and induced mid-gap states of doped NTs considered in this study (Table 2 and Fig. 2) is given in Figs. 3a and 3b (based on results of LCAO and LACW calculations, respectively). In this study we can compare one-electron energy spectra and DOSs after LACW re-scaling only (Subsection 2.3); thus, to achieve their quantitative compatibility with LCAO results, we can put forward consolidated conclusions based on both types of first principles calculations. Both LCAO and LACW calculations show that for the pristine titania nanotube, the values of $\Delta\varepsilon_{gap}$ considerably exceed 4.0 eV (Table 2), which corresponds to the far ultraviolet range of spectrum.

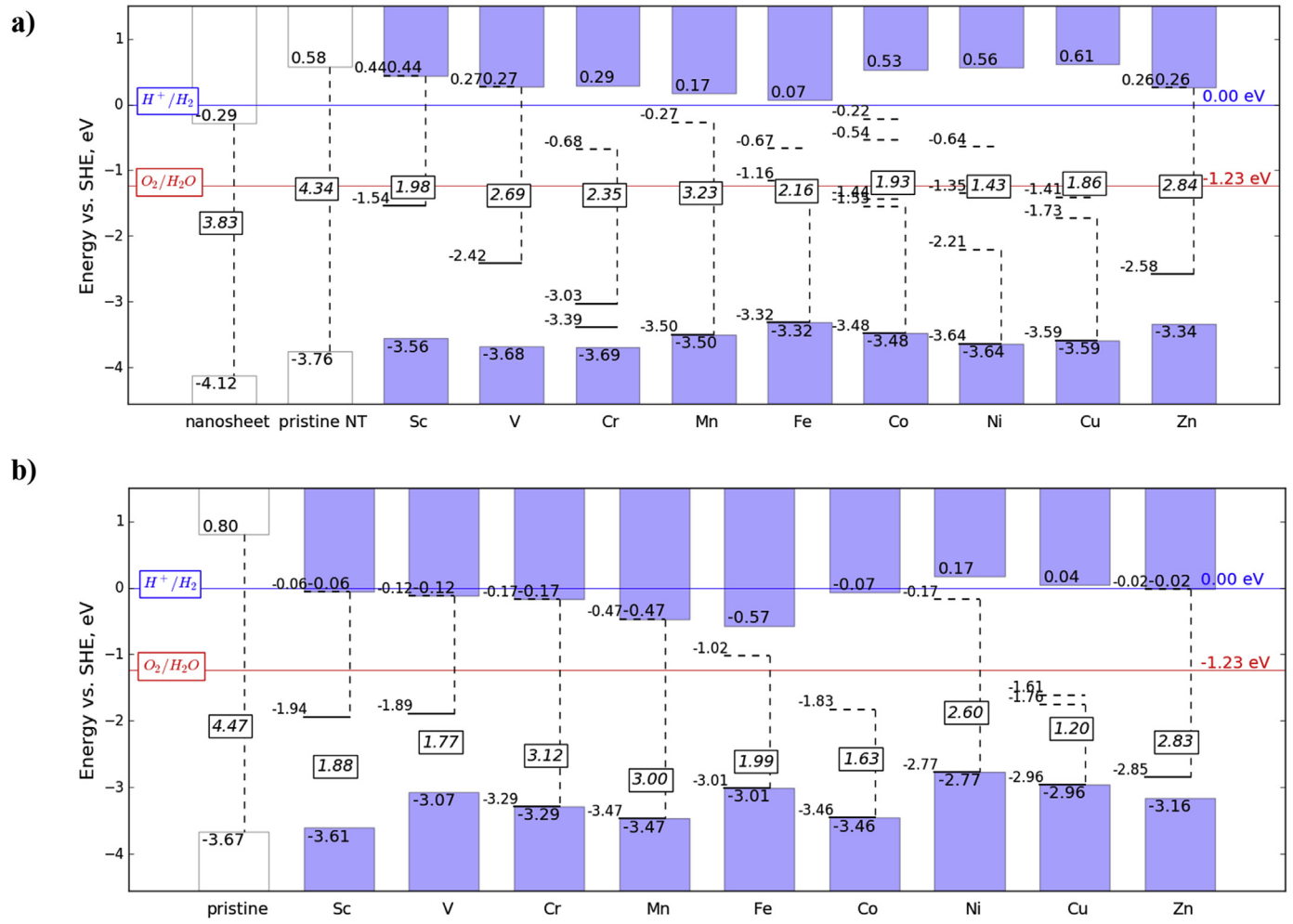


**Fig. 3.** Energy diagrams for pristine and doped fluorite-structured $TiO_2$ nanotubes, calculated using LCAO (a) and LACW (b) methods. The red and blue horizontal dotted lines correspond to the redox potentials, $\varepsilon_{O_2/H_2O}$ and $\varepsilon^{+}_{H/H_2}$, respectively. The zero of the energy scale corresponds to the potential of the standard hydrogen electrode SHE ($\varepsilon^{+}_{H/H_2}$), which explains the difference to the one-electron levels in respect to vacuum zero as presented in Table 2. Solid and dashed horizontal lines describe $\varepsilon_{HOIL}$ and $\varepsilon_{LUIL}$ levels, respectively. Upper rectangles correspond to the conduction bands, while lower filled rectangles stand for the valence bands (the corresponding numbers describe the values of edge energies). (For interpretation of the references to colour in this figure legend, the reader is referred to the web version of this article.)

The best candidate for application in photocatalysis is found to be the fluorite-structured Sc-doped titania nanotube; its band gap calculated using the LCAO and LACW methods are found to be 1.98 and 1.88 eV, respectively, i.e., it corresponds to the yellow or orange ranges of visible spectra, respectively. This result qualitatively agrees with experimental studies of Sc-doped nanoparticles [29]. Another possible candidate for photocatalytic applications is the V-doped titania nanotube; B3LYP-LCAO calculations give $\Delta\varepsilon'_{gap}$ = 2.69 eV (blue-violet range) while the value of 1.77 eV (orange-red range) observed for the reduced band gap obtained in the LDA-LACW calculations is rather an artifact of energy re-scaling (when the bottom of the conduction band is downshifted in majority of plots as shown in Fig. 2IIb-f; therefore, a substantial part at the bottom of the conduction band overlaps in this case with the redox interval, thus leading to electron-hole recombination). We can also predict photocatalytic suitability for Zn-doped $TiO_2$ if the energy level chipped off from the valence band is occupied. Such a possibility is confirmed by experimental studies on Zn-doped titania nanoclusters [55,56] and nanotubes [32]. In this case, values of $\Delta\varepsilon'_{gap}$ correspond to violet area of the visible spectrum. For other 3*d*-metal dopants, either Eq. (2) is not fulfilled (Co and Cu) or the energy levels induced by dopants are positioned inside the redox interval (Cr, Mn, Fe and Ni), which unavoidably leads to electron-hole recombination and thus excludes their photocatalytic suitability.

## 4. Summary

Using both B3LYP-LCAO and LDA-LACW methods, we have performed comprehensive first-principles simulations of single-walled three-layer fluorite-structured $TiO_2$ (4,4) NTs, both pristine and doped by various 3*d* metals. For proper comparison of densities of one-electron states for pristine and doped nanotubes calculated by both methods, including the arrangement of these states along the energy scale, we have re-scaled the DOSs calculated using the LDA-LACW method (Subsection 2.3) to make them qualitatively compatible with those calculated using the B3LYP-LCAO approach, although certain disagreements still remain. Obviously, the energy spectra obtained using the former must therefore be assumed to be less reliable and informative. An evident artifact in LDA–LACW models is the downshift of the bottom of the conduction band.

Nevertheless, when using both computational schemes, the calculated DOSs show the formation of induced mid-gap states in the band gap of doped $TiO_2$ (4,4) NTs, leading to the narrowing of this energy gap ($\Delta\varepsilon_{gap} \rightarrow \Delta\varepsilon'_{gap}$, Table 1). Thus, we can conclude that the presence of 3*d*-metal impurities drastically affects the band structure of titania nanotubes (qualitatively similar for both methods) which must be taken into account when constructing nanoelectronic devices based on such nanotubes.

Analysis of equilibrium distances and Mulliken populations between the substituent and the nearest oxygen atoms demonstrates for the B3LYP-LCAO method that their bond lengths tend to be increasingly elongated with increasing atomic number of the dopant (except for Sc) relative to the Ti–O bond length of the pristine titania nanotube. However, such a growth of the $l_{\text{dopant-O}}$ bonds is not accompanied by reduced covalency to a similar extent as observed by us in BN NTs doped by $s^2p$ metals [49]. This can be explained by the different chemical nature of both types of nanotubes as well as *sp*- and *d*-metal dopants.

Comparison of the band edge positions and Fermi levels relatively to the levels of reduction $H^+/H_2$ (SHE) and oxidation $O_2/H_2O$ potentials, as well as the analysis of the band gap widths allows us to suggest possible configurations of doped $TiO_2$ nanotubes suitable for application in photocatalytic splitting of water molecules under solar irradiation in the visible range. Band engineering of $TiO_2$ (4,4) NTs clearly shows that the $Sc_{Ti}$ substituted nanotube can be considered as a good candidate for photocatalytic applications since its band gap equal to 1.8–1.9 eV, corresponding to orange and yellow range of solar spectrum, possesses a high conversion of solar energy. This doping is also energetically favorable since the formation energy of Sc-doped NT is relatively low (5.92 eV *per* defect) as compared to other 3*d*–metal dopants, for which $E^{form}$ values are increased almost proportionally to their atomic numbers. As alternative dopants, we can also consider V-doped defects, the formation energy of which is even less, namely 5.50 eV, than in the case of Sc.

In our recent studies, we have found that, in the case of anatase-structured $TiO_2$ NTs, the $N_O$ and $S_O$ mono-doped as well as $N_O$+$S_O$ co-doped (001) nanotubes [40] can be considered photocatalytically suitable, whereas in the case of (101) titania nanotubes $N_O$+$S_O$ co-doping does not improve the band positions [42]. Although fluorite-structured titania NTs are extremely thin, always single-walled, and energetically only metastable, our prediction can be useful to determine which approaches should be tried and which ones will very likely be unsuccessful when synthesizing doped materials for nanotubular water splitting photocatalysts.

## Acknowledgements

This study has been supported by the EC ERA.Net RUS Plus project No. 237 WATERSPLIT, Russian Basic Research Foundation No. 16-53-76019, and additionally by the IMIS2 Program (Latvia). The authors are also indebted to R. A. Evarestov and O. Lisovski for stimulating discussions as well as to A. Chesnokov for technical assistance.

## References

[1] A. Fujishima, K. Honda, Electrochemical photolysis of water at a semiconductor electrode, Nature 23 (1972) 37–38.
[2] Z. Zhang, P. Wang, Optimization of photoelectrochemical water splitting performance on hierarchical $TiO_2$ nanotube arrays, Energy Environ. Sci. 5 (2012) 6506–6512.
[3] Y. Xu, W. Zhao, R. Xu, Y. Shi, B. Zhang, Synthesis of ultrathin CdS nanosheets as efficient visible-light-driven water splitting photocatalysts for hydrogen evolution, Chem. Commun. 49 (2013) 9803–9805.
[4] M. Anpo, Use of visible light. Second-generation titanium oxide photocatalysts prepared by the application of an advanced metal ion-implantation method, Pure Appl. Chem. 72 (2000) 1787–1792.
[5] X. Chen, S. Shen, L. Guo, S.S. Mao, Semiconductor-based photocatalytic hydrogen generation, Chem. Rev. 110 (2010) 6503–6570.
[6] M. Pelaez, N.T. Nolan, S.C. Pillai, M.K. Seery, P. Falaras, A.G. Kontos, P.S.M. Dunlop, J.W.J. Hamilton, J.A. Byrnee, K. O'Shea, M.H. Entezari, D.D. Dionysius, A review on the visible light active titanium dioxide photocatalysts for environmental applications, Appl. Catal. B 125 (2012) 331–349.
[7] T. Inoue, T. Okumura, Y. Shimazu, E. Sakai, H. Kumigashira, T. Higuchi, Electrical conductivity of Sc-doped $TiO_2$ thin film prepared by RF magnetron sputtering, Jpn. J. Appl. Phys. 53 (2014) 06JG03.
[8] T. Umebayashi, T. Yamaki, H. Itoh, K. Asai, Analysis of electronic structures of 3*d* transition metal-doped $TiO_2$ based on band calculations, J. Phys. Chem. Solids 63 (2002) 1909–1920.
[9] G. Shao, Electronic structures of manganese-doped rutile $TiO_2$ from first principles, Phys. Chem. C 112 (2008) 18677–18685.
[10] C.D. Valentin, G. Pacchioni, H. Onishi, A. Kudo, Cr/Sb co-doped $TiO_2$ from first principles calculations, Chem. Phys. Lett. 469 (2009) 166–171.
[11] X.G. Hou, A.D. Liu, M.D. Huang, B. Liao, X.L. Wu, First-principles band calculations on electronic structures of Ag-doped rutile and anatase $TiO_2$, Chin. Phys. Lett. 26 (2009) 077106.
[12] M. Guo, J. Du, First-principles study of electronic structures and optical properties of Cu, Ag, and Au-doped anatase $TiO_2$, Phys. B 407 (2012) 1003–1007.
[13] L.K. Zhang, B. Wu, M. Wang, L. Chen, G.X. Ye, T. Chen, H.L. Liu, C.R. Huang, J.L. Li, Crystal, electronic and magnetic structure of Co and Ag doped rutile $TiO_2$ from first-principles calculations, Adv. Mater. Res. 399 (2012) 1789–1792.
[14] Y. Wang, R. Zhang, J. Li, L. Li, S. Lin, First-principles study on transition metal-doped anatase $TiO_2$, Nanoscale Res. Lett. 9 (2014) 46.
[15] C. Li, Y.F. Zhao, Y.Y. Gong, T. Wang, C.Q. Sun, Band-gap engineering of early transition-metal-doped anatase $TiO_2$: first principles calculations, Phys. Chem. Chem. Phys. 16 (2014) 21446–21451.

[16] Yu F. Zhukovskii, S. Piskunov, O. Lisovski, A. Chesnokov, D. Bocharov, First principle evaluation of photocatalytic suitability for $TiO_2$-based nanotubes, in: W. Cao (Ed.), Semiconductor Photocatalysis - Materials, Mechanisms and Applications, InTech Open Access Publishers, Rijeka, Croatia, 2016, pp. 105–133.
[17] J.-C. Xu, M. Lu, X.-Y. Guo, H.-L. Li, Zinc ions surface-doped titanium dioxide nanotubes and its photocatalysis activity for degradation of methyl orange in water, J. Mol. Catal. A 226 (2005) 123–127.
[18] D.V. Bavykin, A.A. Lapkin, P.K. Plucinski, L. Torrente-Murciano, J.M. Friedrich, F.C. Walsh, Deposition of Pt, Pd, Ru and Au on the surfaces of titanate nanotubes, Top. Catal. 39 (2006) 151–160.
[19] D. Eder, I.A. Kinloch, A.H. Windle, Pure rutile nanotubes, Chem. Commun. 13 (2006) 1448–1450.
[20] D. Eder, M. Motta, A.H. Windle, Iron-doped Pt-$TiO_2$ nanotubes for photocatalytic water splitting, Nanotechnology 20 (2009) 055602.
[21] J. Yan, S. Feng, H. Lu, J. Wang, J. Zheng, J. Zhao, L. Li, Z. Zhu, Alcohol induced liquid-phase synthesis of rutile titania nanotubes, Mater. Sci. Eng. B 172 (2010) 114–120.
[22] Q. Meng, J. Wang, Q. Xie, L. Xiao, Nanotubes from rutile $TiO_2$ (110) sheets: formation and properties, J. Phys. Chem. C 114 (2010) 9251–9256.
[23] H.J. Liu, G.G. Liu, G.H. Xie, M.L. Zhang, Z.H. Hou, $Gd^{3+}$, N-codoped trititanate nanotubes: preparation, characterization and photocatalytic activity, Appl. Surf. Sci. 257 (2011) 3728–3732.
[24] D. Bhattacharyya, P.K. Sarswat, M. Islam, G. Kumar, M. Misra, M.L. Free, Geometrical modifications and tuning of optical and surface plasmon resonance behaviour of Au and Ag coated $TiO_2$ nanotubular arrays, RSC Adv. 5 (2015) 70361–70370.
[25] J. Muscat, V. Swamy, N.M. Harrison, First-principles calculations of the phase stability of $TiO_2$, Phys. Rev. B 65 (2002) 224112.
[26] R.A. Evarestov, A.V. Bandura, M.V. Losev, S. Piskunov, Yu F. Zhukovskii, Titania nanotubes modeled from 3- and 6-layered (101) anatase sheets: line group symmetry and comparative ab initio LCAO calculations, Phys. E 43 (2010) 266–278.
[27] R.A. Evarestov, Yu F. Zhukovskii, A.V. Bandura, S. Piskunov, Symmetry and models of single-wall BN and $TiO_2$ nanotubes with hexagonal morphology, J. Phys. Chem. C 114 (2010) 21061–21069.
[28] J.W. Pan, C. Li, Y.F. Zhao, R.X. Liu, Y.Y. Gong, L.Y. Niu, X.J. Liu, B.Q. Chi, Electronic properties of $TiO_2$ doped with Sc, Y, La, Zr, Hf, V, Nb and Ta, Chem. Phys. Lett. 628 (2015) 43–48.
[29] A. Latini, C. Cavallo, F.K. Aldibaja, D. Gozzi, D. Carta, A. Corrias, L. Lazzarini, G. Salviati, Efficiency improvement of DSSC photoanode by scandium doping of mesoporous titania beads, J. Phys. Chem. C 117 (2013) 25276–25289.
[30] M. Hiranow, K. Date, Scandium-doped anatase ($TiO_2$) nanoparticles directly formed by hydrothermal crystallization, J. Am. Ceram. Soc. 88 (2005) 2604–2607.
[31] D.R. Zhang, H.L. Liu, S.Y. Han, W.X. Piao, Synthesis of Sc and V-doped $TiO_2$ nanoparticles and photodegradation of rhodamine-B, J. Ind. Eng. Chem. 19 (2013) 1838–1844.
[32] X. Gao, B. Zhou, R. Yuan, Doping a metal (Ag, Al, Mn, Ni and Zn) on $TiO_2$ nanotubes and its effect on Rhodamine B photocatalytic oxidation, Environ. Eng. Res. 20 (2015) 329–335.
[33] F. Pascale, C.M. Zicovich-Wilson, F. Lopez, B. Civalleri, R. Orlo, R. Dovesi, The calculation of the vibrational frequencies of crystalline compounds and its implementation in the CRYSTAL code, J. Comput. Chem. 25 (2004) 888–897.
[34] R. Dovesi, V. R. Saunders, C. Roetti, R. Orlando, C. M. Zicovich-Wilson, F. Pascale, B. Civalleri, K. Doll, N. M. Harrison, I. J. Bush, Ph. D'Arco, M. Llunell, M. Causá, Y. Noël, *CRYSTAL14 User's Manual* (University of Turin, Turin, 2014), http://www.crystal.unito.it (accessed 02.01.17).
[35] P.N. D'yachkov, Augmented waves for nanomaterials, in: N.S. Nalwa (Ed.), Encyclopedia of Nanoscience and Nanotechnology vol. 1, Amer. Sci. Publishers, 2004, pp. 191–212.
[36] P.N. D'yachkov, Linear augmented cylindrical wave method for nanotubes electronic structure, Int. J. Quant. Chem. 116 (2016) 174–188.
[37] R.A. Evarestov, Yu F. Zhukovskii, A.V. Bandura, S. Piskunov, Symmetry and models of single-walled $TiO_2$ nanotubes with rectangular morphology, Centr. Eur. J. Phys. 9 (2011) 492–501.
[38] R.A. Evarestov, Yu F. Zhukovskii, A.V. Bandura, S. Piskunov, M.V. Losev, Symmetry and models of double-wall BN and $TiO_2$ nanotubes with hexagonal morphology, J. Phys. Chem. C 115 (2011) 14067–14076.
[39] O. Lisovski, S. Piskunov, Yu F. Zhukovskii, J. Ozolins, *Ab initio* modeling of sulphur doped $TiO_2$ nanotubular photocatalyst for water-splitting hydrogen generation, IOP Conf. Ser. Mater. Sci. Eng. 38 (2012) 012057.
[40] S. Piskunov, O. Lisovski, J. Begens, D. Bocharov, Yu F. Zhukovskii, M. Wessel, E. Spohr, C-, N-, S-, and Fe-doped $TiO_2$ and $SrTiO_3$ nanotubes for visible-light-driven photocatalytic water splitting: prediction from first principles, J. Phys. Chem. C 119 (2015) 18686–18696.
[41] A. Chesnokov, O. Lisovski, D. Bocharov, S. Piskunov, Yu F. Zhukovskii, M. Wessel, E. Spohr, Ab initio simulations on N and S co-doped titania nanotubes for photocatalytic applications, Phys. Scr. 90 (2015) 094013.
[42] O. Lisovski, A. Chesnokov, S. Piskunov, D. Bocharov, YuF. Zhukovskii, M. Wessel, E. Spohr, *Ab initio* calculations of doped $TiO_2$ anatase (101) nanotubes for photocatalytical water splitting applications, Mater. Sci. Semicond. process. 42 (2016) 138–141.
[43] A.D. Becke, Density-functional thermochemistry. III. The role of exact Exchange, J. Chem. Phys. 98 (1993) 5648–5652.
[44] P.J. Hay, W.R. Wadt, *Ab initio* effective core potentials for molecular calculations. Potentials for K to Au including the outermost core orbitals, J. Chem. Phys. 82 (1985) 299–310.
[45] F. Weigend, R. Ahlrichs, Balanced basis sets of split valence, triple zeta valence and quadruple zeta valence quality for H to Rn: design and assessment of accuracy, Phys. Chem. Chem. Phys. 7 (2005) 3297–3305.
[46] H.J. Monkhorst, J.D. Pack, Special points for Brillouin-zone integrations, Phys. Rev. B 13 (1976) 5188.
[47] P.N. D'yachkov, D.V. Makaev, Account of helical and rotational symmetries in the linear augmented cylindrical wave method for calculating the electronic structure of nanotubes: towards the *ab initio* determination of the band structure of a (100, 99) tubule, Phys. Rev. B 76 (2007) 195411.
[48] P.N. D'yachkov, D.Z. Kutlubaev, D.V. Makaev, Linear augmented cylindrical wave green's function method for electronic structure of nanotubes with substitutional impurities, Phys. Rev. B 82 (2010) 035426.
[49] Yu F. Zhukovskii, S. Piskunov, J. Kazerovskis, D.V. Makaev, P.N. D'yachkov, J. Phys. Chem. C 117 (2013) 14235–14240.
[50] P.N. D'yachkov, V.A. Zaluev, S.N. Piskunov, Yu F. Zhukovskii, Comparative analysis of the electronic structures of mono- and bi-atomic chains of IV, III–V and II–VI group elements calculated using the DFT LCAO and LACW methods, RSC Adv. 5 (2015) 91751–91759.
[51] Y. Xu, M.A.A. Schoonen, The absolute energy positions of conduction and valence bands of selected semiconducting minerals, Am. Mineral. 85 (2000) 543–556.
[52] C.R.A. Catlow, Z.X. Guo, M. Miskufova, S.A. Shevlin, A.G.H. Smith, A.A. Sokol, A. Walsh, D.J. Wilson, S.M. Woodley, Advances in computational studies of energy materials, Philos. Trans. R. Soc. A 368 (2010) 3379–3456.
[53] T. Bak, J. Nowotny, M. Rekas, C.C. Sorrell, Photo-electrochemical hydrogen generation from water using solar energy. Materials-related aspects, Int. J. Hydrogen Energy 27 (2010) 991–1022.
[54] E. Thimsen, S. Biswas, C.S. Lo, P. Biswas, Predicting the band structure of mixed transition metal oxides: theory and experiment, J. Phys. Chem. C 113 (2009) 2014–2021.
[55] Y. Zhao, C. Li, X. Liu, F. Gu, H.L. Du, L. Shi, Zn-doped $TiO_2$ nanoparticles with high photocatalytic activity synthesized by hydrogen–oxygen diffusion flame, Appl. Catal. B 79 (2008) 208–215.
[56] R. Chauhan, A. Kumar, R.P. Chaudhary, Structural and optical characterization of Zn doped $TiO_2$ nanoparticles prepared by sol–gel method, J. Sol.-Gel. Sci. Technol. 61 (2012) 585–591.